Global Approximations of Unsteady-State Adsorption, Diffusion, and Reaction in a Porous Catalyst

Jietae Lee and Dong Hyun Kim
Dept. of Chemical Engineering, Kyungpook National University, Taegu 702-701, Korea

DOI 10.1002/aic.14014
Published online January 24, 2013 in Wiley Online Library (wileyonlinelibrary.com)

The pore diffusion model that describes unsteady-state adsorption, diffusion, and reaction in a porous catalyst is in the form of a parabolic partial differential equation. To relieve computational loads, approximate ordinary differential equations are often used and they can be derived from the transfer function between the surface and average concentrations in the particle. The transfer function shows half-order behaviors at the high-frequency range. The rational transfer functions cannot describe well this half-order behavior. Here, introducing the half-order term to rational transfer function candidates for approximation, models valid throughout low- and high-frequency ranges are derived. Since the proposed approximate models are valid globally, they can be applied to reactive porous catalysts easily. They can also be used for noninteger shape factors that will show better performances for adsorbents different from ideal geometries of infinite slab, infinite cylinder and sphere, and for biporous adsorbents. © 2013 American Institute of Chemical Engineers *AIChE J*, 59: 2540–2548, 2013

Keywords: porous adsorbent, pore diffusion model, adsorption, diffusion, reaction, fractional order model, linear driving force model

Introduction

Models for practical separation processes such as packed bed adsorbers involve mass balance equations for the bulk flows through the adsorbers in addition to the dynamic mass transfers in adsorbent particles. Both mass balance equations can be represented by partial differential equations. These coupled partial differential equations are rather complicate and the pore diffusion model representing the dynamic mass transfers in the particles need be approximated for reduced computational loads.[1–4]

To approximate the unsteady-state diffusion and adsorption in a spherical adsorbent, Glueckauf[5] proposed a first-order ordinary differential equation named the linear driving force (LDF) model. By assuming that the mass-transfer rate is proportional to the difference between the surface concentration and the average concentration in a particle, the partial differential equation is replaced approximately by the first-order ordinary differential equation. The LDF model can also be derived in several different ways[6–8] such as the orthogonal collocation and the Pade approximation. This simplification is very effective in reducing computational loads. The first-order model for the spherical adsorbent without reaction is extended to other adsorbent geometries without reaction[9] and with the first-order reaction.[10–12] An improved first-order model having the term of the changing rate of surface concentration is available for adsorbents without reaction[10] and with the first-order reaction.[3]

Correspondence concerning this article should be addressed to J. Lee at jtlee@knu.ac.kr.

The LDF model is valid only when the surface concentration of the particle changes slowly. To improve the approximation accuracy, Cruz et al.[13] obtained high-order approximations using the orthogonal collocation method. Lee and Kim[6,14] proposed high-order differential equation models which approximate the pore diffusion model accurately by applying the Pade approximation method to the Laplace domain solution. The Pade method uses the Taylor series of Laplace domain solution and the required number of terms in the Taylor series increases, as the order of approximation increases. Since obtaining high-order terms in the Taylor series becomes quite involved, it is not simple to obtain a high-order approximation by the Pade method, especially when the reaction term is included.[14] Recently, as a useful alternative to the Pade method, an approximation method based on the continued fraction of the Laplace domain solution has been developed.[15] The continued fraction method unifies approximations for slab, cylinder, and sphere adsorbents and the resulting models are systematic. The time-domain differential equations for approximate models of the continued fraction method can be obtained without any involved computation.

The pore diffusion model is infinite dimensional and shows half-order behaviors[16] for a fast varying surface concentration. Hence, each finite dimensional model has its limited valid region and should be used carefully. For a slowly varying surface concentration, a model based on the Pade approximation which shows excellent fitting results around zero frequency can be used. Conversely, for a fast varying surface concentration as in the cyclic adsorption and desorption, a model that fits a high-frequency region of the pore diffusion model should be used. Recently, to avoid this cumbersome, a simple half-order model that is valid for the entire frequency range

has been proposed.[16] Although the half-order model is global, it is less accurate than others such as the Pade approximations for a certain frequency range. Here, we develop globally accurate approximations showing the correct half-order asymptotic behavior at high frequencies as well as high accuracy of the Pade approximations at low frequencies. The proposed simple unified models can be effectively used for the process optimization and model parameter estimations that require many repeated computations.

Mass Balance Equation for the Unsteady-State Diffusion, Adsorption, and Reaction

The mass-transfer rate through an adsorbent surface is dependent on the average concentration in the adsorbent particle. For the average concentration, it is needed to know the concentration profile in the adsorbent particle in detail which will be a function of time and position. The mass balance equation for this is in the form of partial differential equation having many variables. Here, for brevity, the dimensionless mass balance equation with normalized variables is used. Detailed definitions of variables can be found in Kim.[12] The dimensionless mass balance equation for a linear adsorption and a first-order reaction in a catalyst is

$$\begin{aligned} &\frac{\partial q}{\partial t}=\frac{1}{r^{\zeta}}\frac{\partial}{\partial r}\left(r^{\zeta}\frac{\partial q}{\partial r}\right)-\phi^2 q \\ &q(r,0)=0 \\ &\left.\frac{\partial q(r,t)}{\partial r}\right|_{r=0}=0, \qquad q(1,t)=f(t) \end{aligned} \tag{1}$$

Here, r and t are the dimensionless position and time variables, respectively. $q(r, t)$ is the dimensionless concentration in the particle, and $f(t)$ is a time-varying concentration at the adsorbent surface. ϕ is the Thiele modulus. The shape factor ζ is 0 for the infinite slab, 1 for the infinite cylinder, and 2 for the sphere. The volume-average concentration is

$$\bar{q}(t)=(\zeta+1)\int_0^1 r^{\zeta}q(r,t)dr \tag{2}$$

The volume-average concentration $\bar{q}(t)$ is of the main interest because the mass exchange rate between the adsorbent and its surrounding can be conveniently expressed as $d\bar{q}(t)/dt$.

Eqs. 1 with 2 can be solved in the time domain by the separation of variables method.[17] For example, the analytic solution for a sphere catalyst ($\zeta=2$) in the absence of reaction ($\phi=0$) is[18]

$$\bar{q}(t)=6\sum_{k=1}^{\infty}\int_0^t \exp\left(-k^2\pi^2(t-\tau)\right)f(\tau)d\tau \tag{3}$$

When the Laplace transformation method is applied,[17] Eqs. 1 with 2 becomes

$$\begin{aligned} &\frac{d^2Q(r,s)}{dr^2}+\frac{\zeta}{r}\frac{dQ(r,s)}{dr}-\left(s+\phi^2\right)Q(r,s)=0 \\ &\left.\frac{dQ(r,s)}{dr}\right|_{r=0}=0, \quad Q(1,s)=F(s) \end{aligned} \tag{4}$$

and

$$\bar{Q}(s)=(\zeta+1)\int_0^1 r^{\zeta}Q(r,s)dr \tag{5}$$

Here, s is the Laplace variable and $Q(r, s)$, $\bar{Q}(s)$, and $F(s)$ are Laplace transforms of $q(r,t)$, $\bar{q}(t)$, and $f(t)$, respectively. The analytic solution for Eqs. 4 and 5 is[12,15]

$$\begin{aligned} \bar{Q}(s)&=G_{\zeta}\left(s+\phi^2\right)F(s) \\ G_{\zeta}\left(s+\phi^2\right)&=\frac{(\zeta+1)I_{(\zeta+1)/2}\left(\sqrt{s+\phi^2}\right)}{\sqrt{s+\phi^2}I_{(\zeta-1)/2}\left(\sqrt{s+\phi^2}\right)} \\ &=\begin{cases}\dfrac{\tanh\sqrt{s+\phi^2}}{\sqrt{s+\phi^2}}, & \zeta=0 \\ 3\left(\dfrac{1}{\sqrt{s+\phi^2}}\coth\sqrt{s+\phi^2}-\dfrac{1}{s+\phi^2}\right), & \zeta=2\end{cases} \end{aligned} \tag{6}$$

where $G_{\zeta}(s+\phi^2)$ is the transfer function relating the volume-average concentration $\bar{q}(t)$ and the surface concentration $f(t)$. The function $I_a(\cdot)$ in Eq. 6 is the modified Bessel function and right hand side of Eq. 6 can be easily derived from properties of the Bessel functions.[15,19,20]

Expansions and Previous Approximations

It is hard to solve the partial differential equation of Eq. 1 when it is coupled with other balance equations in the form of partial differential equations. There have been many approximate equations to reduce computational loads and almost all the approximate equations can be derived from the Laplace domain solutions of Eq. 6. Here previous works are reviewed.

From properties of Bessel functions,[17,19,20] the transfer function $G_{\zeta}(s)$ can be expanded in various forms as follows;

Taylor series expansion

$$G_{\zeta}(s)=1-\frac{1}{(\zeta+1)(\zeta+3)}s+\frac{2}{(\zeta+1)^2(\zeta+3)(\zeta+5)}s^2+\cdots \tag{7}$$

Continued fraction expansion

$$G_{\zeta}(s)=\frac{\zeta+1}{\zeta+1+\frac{s}{\zeta+3+\frac{s}{\zeta+5+\cdots}}}\equiv\frac{\zeta+1}{\zeta+1+}\frac{s}{\zeta+3+}\frac{s}{\zeta+5+}\cdots \tag{8}$$

Product and partial fraction expansion

$$\begin{aligned} G_{\zeta}(s)&=\prod_{k=1}^{\infty}\left(\frac{s}{z_{k,(\zeta+1)/2^2}}+1\right)\Bigg/\prod_{k=1}^{\infty}\left(\frac{s}{z_{k,(\zeta-1)/2^2}}+1\right) \\ &=2(\zeta+1)\sum_{k=1}^{\infty}\frac{1}{s+z_{k,(\zeta-1)/2^2}}, \qquad z_{k,v}=\text{ roots of } J_v(z) \end{aligned} \tag{9}$$

Asymptotic expansion for a large s

$$G_{\zeta}(s)\approx\frac{\zeta+1}{\sqrt{s}}-\frac{\zeta(\zeta+1)}{2s}+\frac{(\zeta-2)\zeta(\zeta+1)}{8s\sqrt{s}}+\cdots \tag{10}$$

The Pade approximation in the form of $P(s)=(b_0+b_1s+\cdots+b_ms^m)/(1+a_1s+\cdots+a_ns^n)$ is such that its Taylor series is the same as the series (7) up to the term of s^{n+m}. When the Taylor series is given, the Pade approximation can be easily obtained by solving a set of linear equations.[21] For example, the first Pade approximation that fits the Taylor series up to the term of s^1 is

$$G_\zeta(s) \approx \frac{1}{\tau_a s+1}, \quad \tau_a = \frac{1}{(\zeta+1)(\zeta+3)} \tag{11}$$

For $\zeta=2$, it is $G_{\zeta=2}(s) \approx 1/(s/15+1)$ and is equivalent to the time-domain equation[22]

$$\dot{\bar{q}}(t) = 15(f(t)-\bar{q}(t)) \tag{12}$$

This equation is known as the LDF model for the sphere adsorbent without reaction proposed by Glueckauf.[5] It can also be derived in various different ways.[6–8] Despite its limited accuracy, it attracts many attentions due to its simplicity and has been applied to various processes.[2,5,7–10,12]

It is surprising that the continued fraction expansion of the transfer function $G_\zeta(s+\phi^2)$ is so simple like Eq. 8. Properties of Bessel functions can be used to derive the continued fraction expansion.[15] It is well-known that the continued fraction expansion, when truncated, is equivalent to the Pade approximation. For example, the first truncation $G_{\zeta=2}(s) \approx 3/(3+s/5)$ for the sphere adsorbent is equivalent to the LDF model of $G_{\zeta=2}(s) \approx 1/(s/15+1)$. Eq. 8 is better to derive the Pade approximation because it does not need solving a set of linear equations and the corresponding state equation is also better in the numerical point of view[23] than that derived from the transfer function of Pade approximation.

The modified Bessel equation has the infinite number of zeros[19] and from these zeros we can obtain the infinite product (9). The corresponding partial fraction expansion of Eq. 9 can be derived by applying the partial fraction expansion method[17] to the infinite product (9) and the derivative relationship between the Bessel functions. The analytic solution of Eq. 3 in the form of convolution integral is equivalent to the transfer function of $G_{\zeta=2}(s)=6\sum_{k=1}^{\infty} 1/(s+k^2\pi^2)$. This partial fraction series can be truncated and used in computing dynamic response of $\bar{q}(t)$. However, the partial fraction series converges slowly and many terms are needed for use in practice.

The above models are accurate for small s and are effective for a slowly varying $f(t)$. When $f(t)$ is varying fast and so high-frequency components are dominant, responses computed through low-order Pade approximations can have large errors. Due to the same reason, Pade approximations based on $G_\zeta(s)$ cannot be used for $G_\zeta(s+\phi^2)$ with a large ϕ by replacing s to $s+\phi^2$. The Pade approximations obtained from the Taylor series expansion of $G_\zeta(s+\phi^2)$ should be used. The Taylor series of $G_\zeta(s+\phi^2)=G_\zeta(\phi^2)+G_\zeta'(\phi^2)s+\cdots$ and the corresponding Pade approximations have been given in Kim and Lee.[14] They are valid regardless of ϕ. However, expressions for the Taylor series terms such as $G_\zeta''(\phi^2)$ and higher order derivatives are rather involved.[14]

It is well-known that $G_\zeta(s)$ approaches $(\zeta+1)/\sqrt{s}$ for a large s and shows the half-order behaviors. More accurately, the asymptotic expansion valid for a large s is given as Eq. 10. It can be derived from the asymptotic expressions of Bessel functions.[19] For global approximations which are valid regardless of changing rate of $f(t)$, Lee and Kim[16] recently proposed a half-order model

$$G_\zeta(s) \approx \frac{1}{\sqrt{\tau_b s+1}} = \frac{\sqrt{\tau_b s+1}}{\tau_b s+1}, \qquad \tau_b = \frac{2}{(\zeta+1)(\zeta+3)} \tag{13}$$

It satisfies the first two terms of Taylor series (7) and the first term of asymptote (10) approximately. It shows the half-order behavior for a large s.

Proposed Models

The above half-order approximation of Eq. 13 has errors in the asymptote for a large s. Its asymptote for a large s is $\sqrt{(\zeta+1)(\zeta+3)/2}/\sqrt{s}$, whereas the exact asymptote of Eq. 6 is $(\zeta+1)/\sqrt{s}$. They are different when ζ is not 1. To compensate this discrepancy, more terms should be added. Here, inspired from the asymptote (10), we consider approximation models in the form

$$H_{\zeta[m]}(s) = \frac{\sqrt{\alpha s+1}}{s}P(s) - \frac{\zeta(\zeta+1)/2}{s}$$
$$P(s) = \frac{\zeta(\zeta+1)/2 + b_1 s + \cdots + b_n s^n}{1 + a_1 s + \cdots + a_n s^n} \tag{14}$$

For a given ζ and n, Eq. 14 has $2n+1$ unknowns of α, a_k's, and b_k's. One equation to determine these unknowns is for Eq. 14 to satisfy the first term of asymptote (10) for a large s. More specifically, since the leading term in the asymptote of Eq. 14 for a large s is $\sqrt{\alpha} b_n/a_n$, we have

$$\zeta+1 = \frac{\sqrt{\alpha} b_n}{a_n} \tag{15}$$

The remaining $2n$ equations are such that the Taylor series of Eq. 14 is equal to that of Eq. 7 up to $2n$ terms. Let m in Eq. 14 be $2n$, representing the number of Taylor series terms to be matched.

In Eq. 14, $P(s)$ is made to have a factor of $(\alpha s+1)$ in the denominator

$$P(s) = \frac{\tilde{P}(s)}{(\alpha s+1)} = \frac{\zeta(\zeta+1)/2 + b_1 s + \cdots + b_n s^n}{(1+\alpha s)(1+\tilde{a}_1 s + \cdots + \tilde{a}_{n-1} s^{n-1})} \tag{16}$$

Then, we have $2n-1$ unknowns to match both Taylor series. In this case, $m=2n-1$ and Eq. 15 becomes $\zeta+1 = b_n/(\tilde{a}_{n-1}\sqrt{\alpha})$. The resulting approximation is in the form of $H_{\zeta[m]}(s) = \frac{1}{s\sqrt{\alpha s+1}}\tilde{P}(s) - \frac{\zeta(\zeta+1)/2}{s}$.

The above problem to determine unknowns is nonlinear. An iterative procedure to solve this coefficients matching problem can be, for a given ζ and m (if m is odd, $n = (m+1)/2$ and, otherwise, $n=m/2$),

Step 1: Guess α.

Step 2: Calculate the Taylor series of $P(s)=(sG_\zeta(s) + \zeta(\zeta+1)/2)/\sqrt{\alpha s+1}$.

Step 3: Calculate the Taylor series of $\tilde{P}(s)=(1+\alpha s)P(s)$ (Eq. 16) if m is odd.

Step 4: Calculate the Pade approximation of $\tilde{P}(s)$ or $P(s)$.

Step 5: Repeat the Steps 2–4 so that Eq. 15 is met. For this, the bisection method can be applied.[17]

The above iterative procedure can be illustrated with the problem to obtain $H_{\zeta=1[2]}(s)$

$$H_{\zeta=1[2]}(s) = \frac{\sqrt{\alpha s+1}}{s}\frac{1+b_1 s}{1+a_1 s} - \frac{1}{s} \tag{17}$$

Eq. 15 becomes

$$\frac{\sqrt{\alpha} b_1}{a_1} = 2 \tag{18}$$

The Taylor series for $P(s)=(\zeta(\zeta+1)/2+sG_\zeta(s))/\sqrt{\alpha s+1}$ is

Table 1. Proposed Approximations for Slab ($\zeta=0$), Cylinder ($\zeta=1$), and Sphere ($\zeta=2$) Geometries

ζ	m	$H_{\zeta[m]}(s)$	$\tilde{H}_{\zeta[m]}(s)$
0	1	$\dfrac{\sqrt{\left(1-1/\sqrt{3}\right)^2 s+1}}{\left(1-1/\sqrt{3}\right)s+1}$	$\dfrac{\sqrt{\left(1-1/\sqrt{3}\right)^2 s+1}}{\left(1-1/\sqrt{3}\right)s+1}$
	2	$\dfrac{1}{\sqrt{0.0704s+1}}\dfrac{0.1077s+1}{0.4058s+1}$	$\dfrac{0.1064s+1}{\sqrt{0.0690s+1}}\dfrac{1}{0.4053s+1}$
	3	$\dfrac{\sqrt{0.0371s+1}}{0.4053s+1}\dfrac{0.1018s+1}{0.04837s+1}$	$\dfrac{\sqrt{0.0356s+1}}{0.0472s+1}\dfrac{0.1013s+1}{0.4053s+1}$
	4	$\dfrac{1}{\sqrt{0.0228s+1}}\dfrac{0.1014s+1}{0.4053s+1}\dfrac{0.0274s+1}{0.04543s+1}$	$\dfrac{0.0264s+1}{\sqrt{0.0215s+1}}\dfrac{0.1013s+1}{0.4053s+1}\dfrac{1}{0.04503s+1}$
1	1	$\dfrac{2\left(2-\sqrt{2}\right)s+1}{s\sqrt{\left(2-\sqrt{2}\right)^2 s+1}}-\dfrac{1}{s}$	
	2	$\dfrac{\sqrt{0.1045s+1}(1.1304s+1)}{s(0.1827s+1)}-\dfrac{1}{s}$	
	3	$\dfrac{(1.1982s+1)(0.0772s+1)}{s\sqrt{0.0495s+1}(0.1734s+1)}-\dfrac{1}{s}$	
2	1	$\dfrac{3\left(\left(1-1/\sqrt{3}\right)s+1\right)}{s\sqrt{\left(1-1/\sqrt{3}\right)^2 s+1}}-\dfrac{3}{s}$	$\dfrac{3\left(\left(1-1/\sqrt{3}\right)s+1\right)}{s\sqrt{\left(1-1/\sqrt{3}\right)^2 s+1}}-\dfrac{3}{s}$
	2	$\dfrac{3\sqrt{0.0704s+1}(0.4058s+1)}{s(0.1077s+1)}-\dfrac{3}{s}$	$\dfrac{3\sqrt{0.0690s+1}(0.4053s+1)}{s(0.1064s+1)}-\dfrac{3}{s}$
	3	$\dfrac{3(0.4053s+1)(0.04837s+1)}{s\sqrt{0.0371s+1}(0.1018s+1)}-\dfrac{3}{s}$	$\dfrac{3(0.0472s+1)(0.4053s+1)}{s\sqrt{0.0356s+1}(0.1013s+1)}-\dfrac{3}{s}$
	4	$\dfrac{3\sqrt{0.0228s+1}(0.4053s+1)(0.04543s+1)}{s(0.1014s+1)(0.0274s+1)}-\dfrac{3}{s}$	$\dfrac{3\sqrt{0.0215s+1}(0.4053s+1)(0.04503s+1)}{s(0.1013s+1)(0.0264s+1)}-\dfrac{3}{s}$

$$(1+sG_{\zeta=1}(s))/\sqrt{\alpha s+1}=(1+s-s^2/8+\cdots)(1-s\alpha/2+s^2 3\alpha^2/8-\cdots)$$
$$=1+(1-\alpha/2)s+(-1/8-\alpha/2+3\alpha^2/8)s^2+\cdots\approx\frac{1+b_1 s}{1+a_1 s},$$
$$a_1=(1/8+\alpha/2-3\alpha^2/8)/(1-\alpha/2),\qquad b_1=1-\alpha/2+a_1 \tag{19}$$

Hence, Eq. 18 becomes

$$\alpha^{5/2}-6\alpha^2+4\alpha^{3/2}+8\alpha-9\alpha^{1/2}+2=0 \tag{20}$$

It is a fifth-order polynomial for $\alpha^{0.5}$ and can be solved iteratively with an initial guess of α.

When α is given, the Taylor series matching problem (Steps 2–4) is linear and can be solved easily. Recent personal computers and programming languages can accomplish this within a second. A computational code based on the state equation[22] is available on request. Because there is only one variable of α, it is also easy to use symbolic programming languages. Table 1 shows models for three geometries of the slab, cylinder, and sphere.

Explicit Models for $\zeta=0$ and 2

Adsorbents are often in the form of slab ($\zeta=0$) or sphere ($\zeta=2$). Hence, models for these two geometries are especially important. Here, a simpler method to compute approximate models for $\zeta=0$ and 2 is investigated. First, for the slab geometry ($\zeta=0$), Eq. 6 becomes

$$G_{\zeta=0}(s)=\frac{\sinh\sqrt{s}}{\sqrt{s}\cosh\sqrt{s}}=\prod_{k=1}^{\infty}\left(\frac{s}{(k\pi)^2}+1\right)\Big/\left(\frac{s}{((k-1/2)\pi)^2}+1\right) \tag{21}$$

As shown in Table 1, model coefficients for $\zeta=0$ in Eq. 14 are very similar to the first few terms of Eq. 21. For explicit computations of coefficients without iterations, these terms can be used for $P(s)$ in Eq. 14. Consider

$$\tilde{H}_{\zeta=0[m]}(s)=\frac{1}{\sqrt{\alpha s+1}}\frac{\gamma s+1}{\beta s+1}\prod_{k=1}^{n}\left(\frac{s}{(k\pi)^2}+1\right)\Big/\left(\frac{s}{((k-1/2)\pi)^2}+1\right) \tag{22}$$

The series expansion of $\tilde{H}_{\varsigma=0[m]}(s)$ is

$$\tilde{H}_{\varsigma=0[m]}(s)= \begin{cases} 1+\left(\gamma-\frac{\alpha}{2}-\beta+\frac{1}{\pi^2}\sum_{k=1}^{n}\left(\frac{1}{k^2}-\frac{1}{(k-1/2)^2}\right)\right)s+\cdots, & \text{for small s} \\ \left(\frac{\gamma}{\sqrt{\alpha}\beta}\prod_{k=1}^{n}\frac{(k-1/2)^2}{k^2}\right)\frac{1}{\sqrt{s}}+\cdots, & \text{for large s} \end{cases} \tag{23}$$

Hence, for the above expansions to be equal to those of $G_{\zeta=0}(s)$ (Eqs. 7 and 10), we have

$$\gamma-\frac{\alpha}{2}-\beta+\frac{1}{\pi^2}\sum_{k=1}^{n}\left(\frac{1}{k^2}-\frac{1}{(k-1/2)^2}\right)=-\frac{1}{3} \tag{24}$$

$$\frac{\gamma}{\sqrt{\alpha}\beta}\prod_{k=1}^{n}\frac{(k-1/2)^2}{k^2}=1 \tag{25}$$

The above two equations have three unknowns of α, β, and γ, and hence one unknown can be fixed arbitrarily. Especially, for a given β or γ, Eqs. 24 and 25 become quadratic for $\sqrt{\alpha}$ and can be solved analytically. With letting $\gamma=\alpha$, the resulting approximations are in the form of $\tilde{H}_{\varsigma=0[m]}(s)=\frac{\sqrt{\alpha}s+1}{\beta s+1}\prod_{k=1}^{n}\left(\frac{s}{(k\pi)^2}+1\right)/\left(\frac{s}{((k-1/2)\pi)^2}+1\right)$. Differently, with letting $\beta=\frac{1}{(n+1/2)^2\pi^2}$, we have approximations in the form of $\tilde{H}_{\varsigma=0[m]}(s)=\frac{\gamma s+1}{\sqrt{\alpha}s+1}\prod_{k=1}^{n}\left(\frac{s}{(k\pi)^2}+1\right)/\prod_{k=1}^{n+1}\left(\frac{s}{((k-1/2)\pi)^2}+1\right)$.

For the sphere geometry, $G_{\varsigma=2}(s)=3(\sqrt{s}/\tanh\sqrt{s}-1)/s=3(1/G_{\zeta=0}(s)-1)/s$ and approximate equations for $\tilde{H}_{\varsigma=2[m]}(s)$ can be obtained by replacing $G_{\zeta=0}(s)$ to its approximations of $\tilde{H}_{\varsigma=0[m]}(s)$

$$\tilde{H}_{\varsigma=2[m]}(s)=\frac{3}{s}\left(\frac{1}{\tilde{H}_{\varsigma=0[m]}(s)}-1\right) \tag{26}$$

Table 1 shows approximate models for geometries of slab and sphere.

Models with Reaction (Nonzero ϕ):

The proposed models fit both the Taylor series for a small s and the asymptote for a large s. Hence, they will be valid for the whole range of s. Different from previous approximations including Pade approximations, the proposed approximations can be used for adsorptions with reaction by replacing s to $s+\phi^2$. In other words, we can use $H_{\varsigma[m]}(s+\phi^2)$ for $G_{\zeta}(s+\phi^2)$.

In addition, although s is replaced by $s+\phi^2$, the structure of proposed models is not changed and the same simulation technique can be used. For example

$$\begin{aligned} H_{\varsigma[m]}(s+\phi^2) &= \frac{\sqrt{\alpha(s+\phi^2)+1}}{s+\phi^2}P(s+\phi^2)-\frac{\varsigma(\varsigma+1)/2}{s+\phi^2} \\ &= \sqrt{\alpha\phi^2+1}\,\frac{\sqrt{\alpha s/(\alpha\phi^2+1)+1}}{s+\phi^2}P(s+\phi^2)-\frac{\varsigma(\varsigma+1)/2}{s+\phi^2} \end{aligned} \tag{27}$$

Equivalently to $H_{\varsigma[m]}(s)$, $H_{\varsigma[m]}(s+\phi^2)$ consists of the same half-order system with rational transfer function systems.

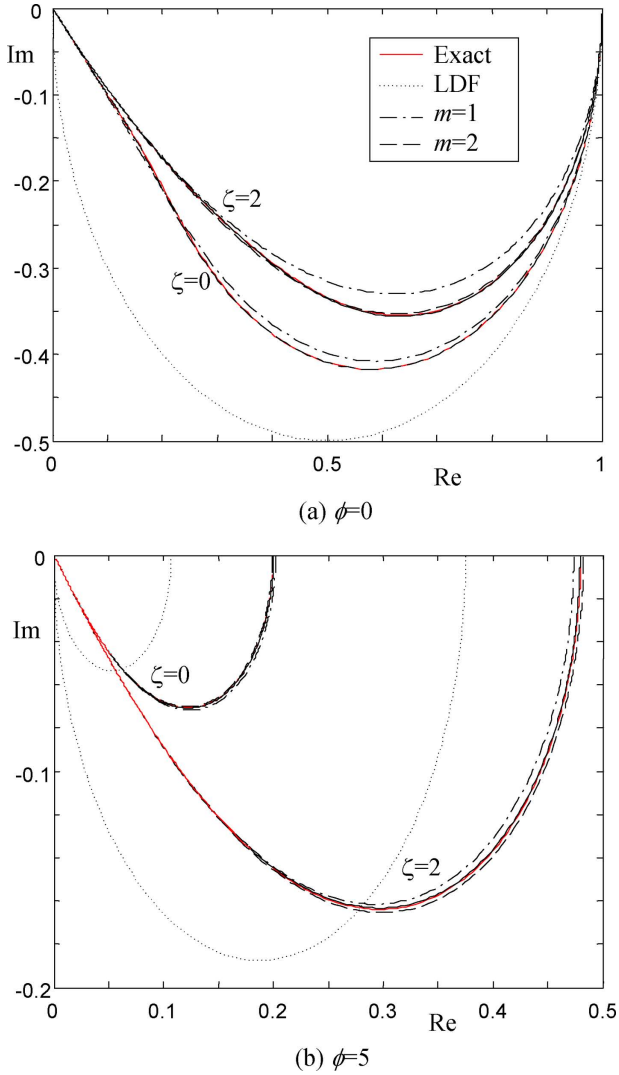

Figure 1. Nyquist plots of the frequency responses of $G_{\zeta}(s+\phi^2)$, LDF model and $\tilde{H}_{\zeta[m]}(s+\phi^2)$.

[Color figure can be viewed in the online issue, which is available at wileyonlinelibrary.com.]

Hence, the same program can be used to simulate. This feature is not valid for the original transfer function of Eq. 6.

Discussions

Approximation accuracies in the frequency domain

Approximation accuracies of proposed models are tested and compared with the LDF model. For this, the fitting accuracies along the imaginary line, $G_{\zeta}(j\omega)$, and the positive real line, $G_{\zeta}(\phi^2)$, are compared. The $G_{\zeta}(j\omega)$ is known as the frequency response. The response for the sinusoidal input $f(t)=\sin(\omega t)$ becomes $\bar{q}(t)=|G_{\zeta}(j\omega)|\sin(\omega t+\angle G_{\zeta}(j\omega))$ at the cyclic steady state. Hence, for a fast varying $f(t)$, models should fit as large value of the angular frequency ω as possible. Conversely, $G_{\zeta}(\phi^2)$ is the steady state gain of the adsorption process with reaction. Fitting accuracies for both $G_{\zeta}(j\omega)$ and $G_{\zeta}(\phi^2)$ will show whether models of $G_{\zeta}(s)$ without reaction can be used as models with reaction by replacing s to $s+\phi^2$.

Figure 1a shows plots of $G_{\zeta}(j\omega)$ and its approximate models in the complex plane (Nyquist plot) for $\zeta=0$ and 2. The Nyquist plots for the LDF models (11) of $\zeta=0$ and 2 appear identical because the frequency ω is not shown explicitly.

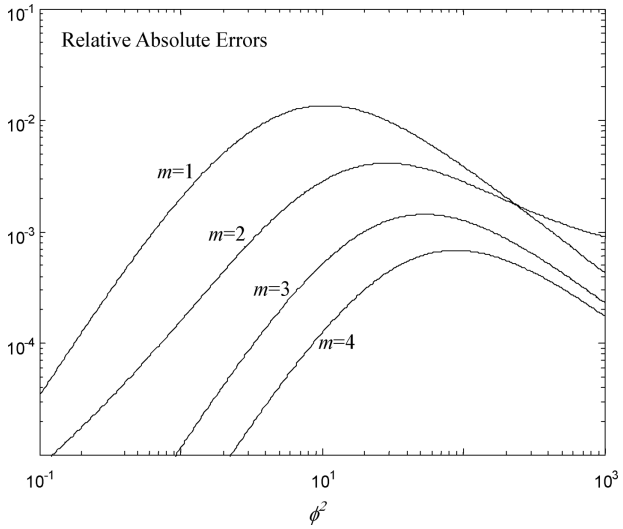

Figure 2. Relative absolute errors of the steady state gains for the slab adsorbent with reaction ($|\tilde{H}_{\zeta=0}(\phi^2)-G_{\zeta=0}(\phi^2)|/|G_{\zeta=0}(\phi^2)|$).

Except for low range of ω, they are much different from the exact frequency responses. For the slab geometry, the maximum absolute relative errors of frequency responses ($\max_\omega|\tilde{H}_\zeta(j\omega)-G_\zeta(j\omega)|/|G_\zeta(j\omega)|$) are 3.6, 1.1, 0.4, and 0.2% for $\tilde{H}_{\zeta=0[m]}(j\omega)$ with m between 1 and 4, respectively. For the sphere geometry, the maximum absolute relative errors of frequency responses are 4.4, 1.3, 0.4, and 0.2% for $\tilde{H}_{\zeta=2[m]}(j\omega)$ with m between 1 and 4, respectively. The LDF models for both geometries show that the maximum absolute relative errors of frequency responses are arbitrarily large.

Figure 1b shows plots of $G_\zeta(j\omega+\phi^2)$ for $\phi=5$ and its approximate models in the complex plane for $\zeta=0$ and 2. The Nyquist plots for the LDF models (11) with replacing s to $s+\phi^2$ for $\zeta=0$ and 2 do not approximate the frequency responses even for low-frequency ranges of ω. The absolute relative errors at $\omega=0$ (steady state gain error) for the LDF models are 46 and 22% for $\zeta=0$ and 2, respectively. These can be made zero by using the first-order model based on the Taylor series expansion of $G_\zeta(s+\phi^2)$.[14] For the slab geometry, the maximum absolute relative errors of frequency responses are 1.1, 0.5, 0.2, and 0.1% for $\tilde{H}_{\zeta=0[m]}(j\omega+\phi^2)$ with m between 1 and 4, respectively. For the sphere geometry, the maximum absolute relative errors of frequency responses are 1.3, 0.6, 0.3, and 0.1% for $\tilde{H}_{\zeta=2[m]}(j\omega+\phi^2)$ with m between 1 and 4, respectively. This figure shows that the reaction term ϕ does not make the proposed approximate model accuracies be worse.

Figure 2 shows the absolute relative errors of approximate models of the slab geometry ($\zeta=0$) for $s=\phi^2$. The maximum absolute relative errors are 1.4, 0.4, 0.1, and 0.07% for $\tilde{H}_{\zeta=0[m]}(\phi^2)$ with m between 1 and 4, respectively. For the sphere geometry, the maximum absolute relative errors are 2.0, 0.5, 0.2, and 0.08% for $\tilde{H}_{\zeta=2[m]}(\phi^2)$ with m between 1 and 4, respectively. Figures 1–2 show that the proposed approximate models will be valid for the whole range of $s=j\omega+\phi^2$.

Time-domain simulations

Figure 3 shows the structure of the proposed models. The time-domain simulation of the half-order part

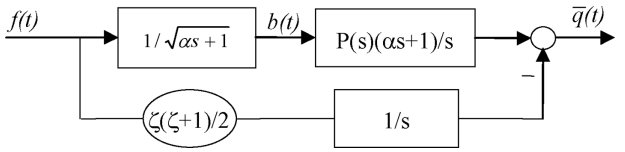

Figure 3. The structure of proposed models for simulations.

$$B(s)=\frac{1}{\sqrt{\alpha s+1}}F(s) \tag{28}$$

is needed. Other parts in Figure 3 can be realized by differential equations.[22] The time response for Eq. 28 can be realized by the convolution integral as

$$b(t)=\frac{1}{\sqrt{\alpha\pi}}\int_0^t\frac{1}{\sqrt{\tau}}e^{-\tau/\alpha}f(t-\tau)d\tau \tag{29}$$

When $f(t)$ is known, Eq. 29 can be integrated analytically. For example, $b(t)=erf\left(\sqrt{t/\alpha}\right)$ for the unit step input of $f(t)=1$.

Figure 4 shows step responses for sphere geometry ($\zeta=2$). The integral of absolute errors (IAE) for adsorption without reaction ($\phi=0$) are 8.8E-3, 7.9E-4, and 1.4E-4 for $\tilde{H}_{\zeta=2[m]}(s)$ with m between 1 and 3, respectively. That of LDF model is 1.6E-2. The IAE for adsorption with reaction ($\phi=5$) are 2.9E-3, 1.2E-3, and 3.5E-4 for $\tilde{H}_{\zeta=2[m]}(s+\phi^2)$ with m between 1 and 3, respectively. The IAE values decrease by approximately an order of magnitude as the approximation order increases. That of LDF model with $s+\phi^2$ instead of s is 5.5E-2.

The convolution integral of Eq. 29 is inconvenient for a general input $f(t)$. This half-order element can be further approximated. Many methods for this are available. For example, consider the continued fraction of half-order system[19]

$$1/\sqrt{s+1}=\frac{1}{1+}\frac{s}{2+}\frac{s}{2+}\frac{s}{2+}\cdots \tag{30}$$

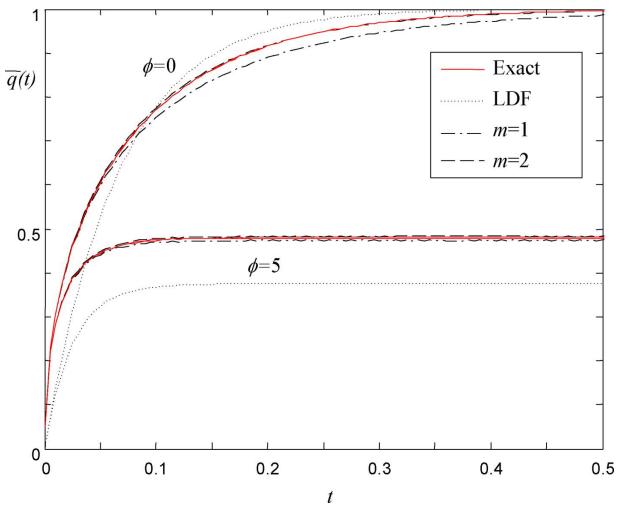

Figure 4. Step responses of $G_{\zeta=2}(s+\phi^2)$, LDF model, and $\tilde{H}_{\zeta=2[m]}(s+\phi^2)$.

[Color figure can be viewed in the online issue, which is available at wileyonlinelibrary.com.]

From this continued fraction expansion, Pade approximations are obtained easily and Pade approximations of orders around three provide almost exact step responses. Furthermore, reduced order models by applying model reduction technique to higher order Pade approximations[23] can be obtained and used for finding time responses conveniently. Zig-zag line approximations[24] of frequency response are also available for fast varying inputs.

Application to biporous catalysts and noninteger shape factor ζ

Consider the diffusion and adsorption in a spherical pellet with a biporous structure. The pellet is assumed to be made of spherical porous particles. In the adsorbent, the adsorbate diffuses into the adsorbent interior through the macropores and then into the microparticles. Under some assumptions, the mass balance equations are[25,26]

Macropore

$$\varepsilon_a \frac{\partial C_a}{\partial t} = \varepsilon_a D_a \frac{1}{r_a^2}\frac{\partial}{\partial r_a}\left(r_a^2 \frac{\partial C_a}{\partial r_a}\right) - \frac{3(1-\varepsilon_a)}{R_a} D_b \frac{\partial C_b}{\partial r_b}\bigg|_{r_b=R_b} \tag{31}$$

Micropore

$$\frac{\partial C_b}{\partial t} = D_b \frac{1}{r_b^2}\frac{\partial}{\partial r_b}\left(r_b^2 \frac{\partial C_b}{\partial r_b}\right) \tag{32}$$

Initial conditions

$$C_a(r_a,t)|_{t=0}=0, \quad C_b(r_a,r_b,t)|_{t=0}=0 \tag{33}$$

Boundary conditions

$$\begin{aligned} &\frac{\partial C_a}{\partial r_a}|_{r_a=0}=0, \qquad \frac{\partial C_b}{\partial r_b}|_{r_b=0}=0 \\ &C_a(R_a,t)=f(t), \qquad C_b(r_a,R_b,t)=C_a(r_a,t) \end{aligned} \tag{34}$$

Here, C_a and C_b are concentrations, D_a and D_b are diffusivities, ε_a is the macropore porosity, R_a and R_b are radii, r_a and r_b are the radius variables, t is the time variable, the subscript a means variables in macropore, and the subscript b means variables in micropore. This model can describe adsorption dynamics in detail and can be applied to adsorbents such as zeolite crystals and carbon molecular sieves.[25,26] However, it has been rarely used in practice because of its mathematical complexity and bulky numerical computations. This is one of examples that approximations are required.

The transfer function between the dimensionless volume average concentration $\bar{q}(t)$ and the surface concentration $f(t)$ is[26]

$$\begin{aligned} G_{bi}(s) &= \frac{\varepsilon_a H_a}{\varepsilon_a+(1-\varepsilon_a)K}\frac{3\left(\sqrt{G_b(s)}\coth\left(\sqrt{G_b(s)}\right)-1\right)}{s} \\ G_b(s) &= \frac{s}{H_a}\left(1+\frac{3(1-\varepsilon_a)K}{\varepsilon_a}\frac{H_b}{s}\left(\sqrt{s/H_b}\coth\left(\sqrt{s/H_b}\right)-1\right)\right) \end{aligned} \tag{35}$$

where $H_a=D_a/\left(\varepsilon_a R_a^2\right)$, $H_b=D_b/R_a^2$ and K is the dimensionless adsorption constant. The Taylor series expansion and corresponding approximate models by the Pade method have been proposed by Kim and Lee.[26]

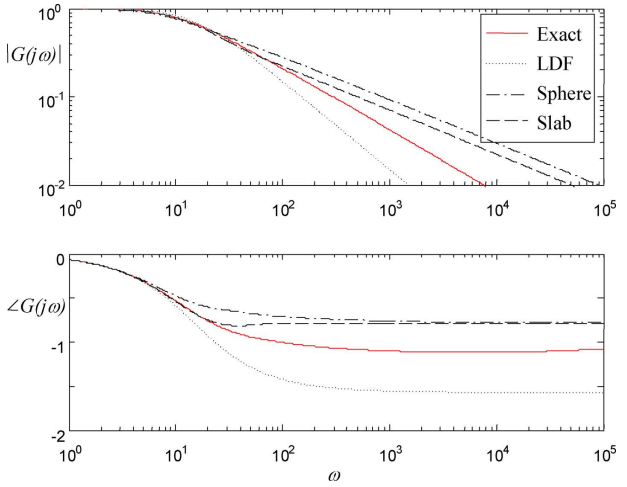

Figure 5. Bode plots of the biporous system (H_a=400, H_b=2.404, ε_a=0.3, and K=100) and its approximations of the LDF model, the monoporous models with sphere and slab geometries.

[Color figure can be viewed in the online issue, which is available at wileyonlinelibrary.com.]

The simplest first-order model (LDF model) is

$$\begin{aligned} G_{bi}(s) &\approx \frac{1}{\tau_a s+1} \\ \tau_a &= \frac{1}{15}\left(\frac{\varepsilon_a+(1-\varepsilon_a)K}{\varepsilon_a H_a}+\frac{(1-\varepsilon_a)K}{H_b(\varepsilon_a+(1-\varepsilon_a)K)}\right) \end{aligned} \tag{36}$$

When the time variable is scaled to be

$$\left(\frac{\varepsilon_a+(1-\varepsilon_a)K}{\varepsilon_a H_a}+\frac{(1-\varepsilon_a)K}{H_b(\varepsilon_a+(1-\varepsilon_a)K)}\right)=1 \tag{37}$$

Eq. 36 becomes the LDF equation of Eq. 8 for a monoporous diffusion with the sphere geometry $(\tau_a=1/((\zeta+1)(\zeta+3))_{\zeta=2}=1/15)$. This provides an overall effective diffusivity[25] that represents two diffusivities of biporous diffusion by one approximately. In principle, the monoporous diffusion model and the biporous diffusion model are incompatible with each other. Nevertheless, the simpler monoporous model is very useful. In the previous works, the sphere geometry is used preferentially because the external shape of adsorbent is sphere. Here, other geometry is shown to be better for some cases.

If the time is scaled to be

$$\left(\frac{\varepsilon_a+(1-\varepsilon_a)K}{\varepsilon_a H_a}+\frac{(1-\varepsilon_a)K}{H_b(\varepsilon_a+(1-\varepsilon_a)K)}\right)=5 \tag{38}$$

Eq. 38 becomes $G_{bi}(s)\approx 1/(s/3+1)$ and it is the LDF model for the slab geometry $(\tau_a=1/((\zeta+1)(\zeta+3))_{\zeta=0}=1/3)$. Figure 5 shows the Bode plots for the biporous model (35) (H_a=400, H_b=2.404, ε_a=0.3, and K=100), the LDF model (36), the monoporous sphere model (6) with the overall effective diffusivity of Eq. 37[25] and the monoporous slab model (6) with the overall effective diffusivity of Eq. 38. The LDF model is independent on ζ. We can see that the monoporous model with the slab geometry (ζ=0) shows far

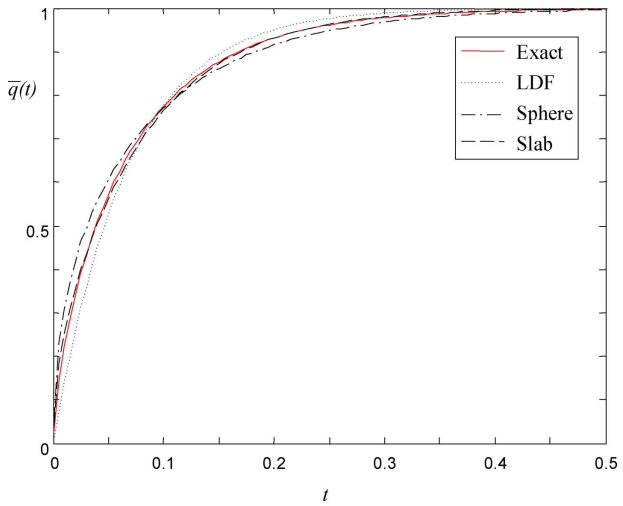

Figure 6. Step responses of the biporous system (H_a=400, H_b=2.404, ε_a=0.3, and K=100) and its approximations of the LDF model, the monoporous models with sphere and slab geometries.

[Color figure can be viewed in the online issue, which is available at wileyonlinelibrary.com.]

better approximations than the other two approximate models. Because the external shape of pellet is sphere, the sphere geometry can be a first choice. The slab geometry, however, is better in this case. The step responses in Figure 6 prove this. The IAE are 8.4E-3, 7.6E-3, and 2.3E-3 for the LDF model, the monoporous sphere models with the overall effective diffusivity of Eq. 37 and the monoporous slab model with the overall effective diffusivity of Eq. 38, respectively.

The shape factor (ζ) can be used as a design parameter. For this, our models are especially adequate since they are not limited to usual three integer values of ζ. There are many examples, including the above biporous catalysts, where noninteger shape factors are needed. For catalysts in the form of the cylindrical pellets with finite length, shape factors with noninteger values between 1 and 2 can provide better approximations.[9] Especially, when the equivalent catalyst radius given by the equation of $R_e=3V/S$, where V and S are the catalyst volume and surface area, is used, the optimal shape factor is evidently noninteger. Our approximate models with noninteger shape factors are helpful to identify the optimal shape factor.

Conclusion

The diffusion and adsorption dynamics in a porous adsorbent can be described in detail by the pore diffusion model in the form of partial differential equation. When this pore diffusion model is coupled with the partial differential equations of bulk flow, its computation is rather involved. To relieve the computational load, approximate models in the form of a set of ordinary differential equations are often used. These approximate differential equations can be derived from the Laplace domain solution. For this, the Pade approximations are especially useful. They are accurate for low-frequency ranges and hence effective for slowly varying surface concentration changes. However, the transfer function for the pore diffusion model shows the half-order behavior for high-frequency ranges and the rational transfer functions of Pade approximations cannot describe this half-order behavior. Here, by introducing the half-order transfer function, approximate equations that are valid globally are obtained. They are in the form of

$$H_{\varsigma[m]}(s)=\frac{\sqrt{\alpha s+1}}{s}P(s)-\frac{\varsigma(\varsigma+1)/2}{s}$$

where $P(s)$ is a rational transfer function of the Laplace variable s. Their approximation accuracies are shown by simulation in the frequency domain and time domain. By replacing s to $s+\phi^2$, the model can be used for porous catalysts with the first-order reactions.

The proposed approximate models can be used for noninteger shape factors different from three integer values of 0 (infinite slab), 1 (infinite cylinder), and 2 (sphere). There are many examples showing that noninteger shape factors provide better performances and the proposed models with noninteger shape factors can be effectively used to solve such problems.

Notation

a_k = coefficient of the denominator polynomial of $P(s)$
b_k = coefficient of the numerator polynomial of $P(s)$
$b(t)$, $B(s)$ = output of a half-order system of Eq. 29 and its Laplace transform
C_a, C_b = concentrations in the macropore and micropore, respectively
D_a, D_b = diffusivities in the macropore and micropore, respectively
$erf(\cdot)$ = error function
$f(t)$, $F(s)$ = dimensionless concentration at the adsorbent surface and its Laplace transform
$G_b(s)$ = transfer function in Eq. 35
$G_{bi}(s)$ = transfer function between $\bar{Q}(s)$ and $F(s)$ for the biporous catalyst
$G_\zeta(s)$, $G_\zeta(s+\phi^2)$ = transfer functions between $\bar{Q}(s)$ and $F(s)$
H_a, H_b = dimensionless constants for $G_{bi}(s)$
$H_{\zeta[m]}(s), \bar{H}_{\zeta[m]}(s)$ = approximation of $G_\zeta(s)$ whose Taylor series expansion is equal to the mth term
$I_a(\cdot)$ = modified Bessel function
K = dimensionless adsorption constant
$P(s)$, $\tilde{P}(s)$ = rational polynomials of s
$q(r,t)$, $Q(r,s)$ = dimensionless concentration in the particle and its Laplace transform
$\bar{q}(t), \bar{Q}(s)$ = average of $q(r,t)$ and its Laplace transform
r = dimensionless space variable
r_a, r_b = radius variables in the macropore and micropore, respectively
R_a, R_b = radii in the macropore and micropore, respectively
R_e = equivalent radius
s = Laplace variable
S, V = surface area and volume of a catalyst
t = dimensionless time variable
$z_{k,v}$ = zeros of the Bessel function $J_v(z)$

Greek letters

α, β, γ = constants for $H_{\zeta[m]}(s)$ and $\bar{H}_{\zeta[m]}(s)$
ε_a = macropore porosity
ϕ = Thiele modulus
τ_a = time constant for a first-order system
τ_b = time constant for a half-order system
ζ = shape factor (0: infinite slab, 1: infinite cylinder, 2: sphere)

Subscript

k = kth element

Acknowledgments

This work (2011-001381) was supported by Mid-career Researcher Program through NRF grant funded by the MEST.

Literature Cited

1. Delgado JA, Uguina MA, Sotelo JL, Ruız B. Modelling of the fixed-bed adsorption of methane/nitrogen mixtures on silicalite pellets. *Sep Purif Technol*. 2006;50:192–203.
2. Gomes PS, Leao CP, Rodrigues AE. Simulation of true moving bed adsorptive reactor: detailed particle model and linear driving force approximations. *Chem Eng Sci*. 2007;62:1026–1041.
3. Kim DH. Approximations for unsteady-state diffusion and reaction in porous catalyst and their application to packed-bed reactor. *AIChE J*. 2008;54:2423–2431.
4. Dantas TLP, Luna FMT, Silva IJ Jr, de Azevedo DCS, Grande CA, Rodrigues AE, Moreira RFPM. Carbon dioxide-nitrogen separation through adsorption on activated carbon in a fixed bed. *Chem Eng J*. 2011;169:11–19.
5. Glueckauf E. Theory of chromatography part 10—formulae for diffusion into spheres and their application to chromatography. *Trans Faraday Soc*. 1955;51:1540–1551.
6. Lee J, Kim DH. High-order approximations for noncyclic and cyclic adsorption in a particle. *Chem Eng Sci*. 1998;53:1209–1221.
7. Serbezov A, Sotirchos SV. On the formulation of linear driving force approximations for adsorption and desorption of multicomponent gaseous mixtures in sorbent particle. *Sep Purif Technol*. 2001;24:343–367.
8. Cruz P, Magalhaes FD, Mendes A. Generalized linear driving force approximation for adsorption of multicomponent mixtures. *Chem Eng Sci*. 2006;61:3519–3531.
9. Patton A, Crittenden BD, Perera SP. Use of the linear driving force approximation to guide the design of monolithic adsorbents. *Chem Eng Res Des*. 2004;82:999–1009.
10. Kim DH. Linear driving force formulas for diffusion and reaction in porous catalyst. *AIChE J*. 1989;35:343–346.
11. Szukiewicz MK. New approximate model for diffusion and reaction in a porous catalyst. *AIChE J*. 2000;46:661–665.
12. Kim DH. Linear driving force formulas for unsteady-state diffusion and reaction in slab, cylinder and sphere catalysts. *AIChE J*. 2009;55:834–839.
13. Cruz P, Mendes A, Magalhaes FD. High-order approximations for intra-particle mass transfer. *Chem Eng Sci*. 2004;59:4393–4399.
14. Kim DH, Lee J. High-order approximations for unsteady-state diffusion and reaction in slab, cylinder and sphere catalyst. *Korean J Chem Eng*. 2012;29:42–48.
15. Lee J, Kim DH. Simple high-order approximations for unsteady-state diffusion, adsorption and reaction in a catalyst: a unified method by a continued fraction for slab, cylinder and sphere geometries. *Chem Eng J*. 2011;173:644–650.
16. Lee J, Kim DH. A half-order approximation for the adsorption dynamics in a porous particle. *AIChE J*. 2011;57:2282–2286.
17. Kreyszig E. Advanced Engineering Mathematics. New York: Wiley, 1999.
18. Carslaw HS, Jaeger JC. Conduction of Heat in Solids. Oxford: Oxford University Press, 1959.
19. Abramowitz M, Stegun IA. Handbook of Mathematical Functions. New York: Dover Publication, 1972.
20. Watson GN. A Treatise on the Theory of Bessel Functions, 2nd ed. New York: Cambridge University Press, 1952.
21. Bender CM, Orszag SA. Advanced Mathematical Methods for Scientists and Engineers. New York: McGraw-Hill, 1978.
22. Kailath T. Linear Systems. New Jersey: Prentice-Hall, 1980.
23. Cho W, Lee J. Applications of high order approximations for unsteady-state diffusion and reaction in a catalyst. *Korean J Chem Eng*. 2012. doi: 10.1007/s11814-012-0188-8.
24. Charef A, Sun HH, Tsao YY, Onaral B. Fractal system as represented by singularity function. *IEEE Trans Automat Control*. 1992;37:1465–1470.
25. Kim DH. A new linear approximation formula for cyclic adsorption in a biporous adsorbent. *Chem Eng Sci*. 1997;52:3471–3482.
26. Kim DH, Lee J. High-order approximations for noncyclic and cyclic adsorption in a biporous adsorbent. *Korean J Chem Eng*. 1999;16:69–74.

Manuscript received Sept. 9, 2012, and revision received Dec. 12, 2012.